Narrowing of the palladium-hydrogen miscibility gap in nanocrystalline palladium

J. A. Eastman, L. J. Thompson, and B. J. Kestel
Argonne National Laboratory, Materials Science Division, Argonne, Illinois 60439-4838
(Received 12 November 1992; revised manuscript received 22 March 1993)

In situ x-ray-diffraction studies of the hydriding behavior of coarse-grained and nanocrystalline palladium samples at ambient temperature are descibed. A previously observed narrowing of the miscibility gap in nanocrystalline palladium was reproduced. The present results, however, demonstrate that this change in the palladium-hydrogen phase diagram for nanocrystalline material is not related to an inability to form the hydride phase in highly disordered grain boundary regions as previously proposed. Instead, the entire volume of nanocrystalline samples was observed to transform to β-PdH upon exposure to hydrogen. This behavior indicates that the entropy and/or enthalpy of mixing for the palladium-hydrogen system differs in nanocrystalline and coarse-grained materials. Because of these changes in thermodynamic quantities, the phase boundary of the palladium-hydrogen miscibility gap is predicted to be shifted to lower temperatures for nanocrystalline samples.

I. INTRODUCTION

Nanocrystalline materials with typical grain sizes of less than 20 nm possess many properties that differ from those of conventional coarser-grained material (for recent reviews, see Refs. 1 and 2). One example where the properties of a material have been reported to change significantly with decreasing grain size is the hydriding behavior of palladium.[3] Property differences between nanocrystalline and coarse-grained materials, including differences in hydriding behavior, have generally been attributed to the fact that a very large fraction of the atoms in nanocrystalline materials are located quite close to grain boundaries (approximately 50% of the atoms in 5-nm-grained-sized material are within 0.5 nm of one or more grain boundaries). Thus, to understand property modifications in nanocrystalline materials, it is important to characterize the structure of their grain boundaries.

Studies of grain-boundary structure in nanocrystalline materials have been controversial. Early reports, based on x-ray-diffraction investigations of nanocrystalline iron[4] and extended x-ray-absorption fine-structure (EXAFS) investigations of copper and palladium,[5] proposed that interfaces in nanocrystalline materials are highly disordered. In the case of nanocrystalline iron, it was concluded that grain-boundary atoms are displaced in random directions from normal lattice sites by up to 50% of a nearest-neighbor distance.[4] More recent studies, using high-resolution microscopy[6] and x-ray diffraction,[7,8] demonstrated that this structural model does not hold for grain boundaries in nanocrystalline palladium. Instead, the evidence suggests that the atomic displacements in nanocrystalline palladium grain-boundary regions are extremely small in magnitude and may be constrained by the close proximity of other boundaries.

The palladium-hydrogen phase diagram contains a miscibility gap below 570 K.[9] Recently, Mütschele and Kirchheim reported that the width of this miscibility gap at 333 K differs for nanocrystalline and coarse-grained palladium samples.[3] They observed that the dilute hydrogen concentration α-PdH phase has a maximum solubility (α_{max}) that is increased by approximately a factor of 2 in 8-nm-grain-sized nanocrystalline palladium compared to that in conventional coarse-grained palladium, while the minimum hydrogen concentration of the β-PdH phase (β_{min}) is reduced by approximately 25% in nanocrystalline palladium compared to coarse-grained material. The increase in α_{max} for nanocrystalline palladium was explained in terms of an increase in hydrogen solubility at the grain boundaries,[3] while the decrease in β_{min} was proposed to be due to a highly disordered grain-boundary structure previously suggested for nanocrystalline materials.[4,5] It was postulated that the grain-boundary regions, which were estimated to occupy 27% of the sample volume, could not be transformed to β-PdH because of their disordered structure. If the grain interiors had the same β_{min} hydrogen concentration as coarse-grained material but the grain boundaries were restricted to have hydrogen concentrations equal to the grain boundary α-phase solubility, this model would predict a decrease in the average hydrogen content in a sample at β_{min} with decreasing grain size or increasing total grain-boundary volume, as observed. Support for this model was provided by comparison with the observed resistance to hydriding of amorphous metals.[10] There was, however, no direct microstructural evidence that a portion of the sample remained untransformed to the β phase.

The disordered grain-boundary structural model offered by Mütschele and Kirchheim to explain their observations is inconsistent with recent studies in which it has been demonstrated that nanocrystalline palladium grain-boundary regions are not highly disordered.[6-8] Therefore it is important to determine whether an alternative explanation exists for the differences in the hydriding behavior of nanocrystalline and coarse-grained palladium. Since x-ray diffraction gives structural information, this technique can be used to monitor the sample microstructure directly during the hydriding phase transition. The goals of the present work were to use *in situ* x-ray-diffraction measurements to (1) verify the existence of a change in the miscibility gap of the palladium-

0163-1829/93/48(1)/84(9)/$06.00

hydrogen system, (2) determine whether a significant volume fraction of nanocrystalline palladium samples resists transformation to the β-PdH phase upon exposure to hydrogen, and (3) develop a self-consistent theory to explain any observed changes in hydriding behavior for nanocrystalline palladium. Preliminary results have been described in a previous report.[11]

II. EXPERIMENTAL METALS

Three nanocrystalline samples (denoted $N1$, $N2$, and $N3$) and one coarse-grained reference sample (denoted CG) were examined in this study. The nanocrystalline samples were produced by evaporating 99.997%-pure palladium wire from a ceramic, resistance-heated evaporation source in an environment consisting of 500 Pa of 99.9999%-pure helium. This process results in the condensation of ultrafine particles[12–14] that are collected and consolidated under vacuum conditions, as first suggested by Gleiter.[15] A consolidation pressure of 1.4 GPa was applied at ambient temperature, resulting in typical sample densities of 80–95 % of the literature value for palladium [12.02 g/cm^3 (Ref. 16)]. The samples were disk shaped with 9 mm diameters and typical thicknesses of 0.1–0.3 mm. The coarse-grained palladium reference sample was cut from a 0.1-mm-thick 99.9957%-pure foil into a 9-mm-diameter disk. The coarse-grained sample was annealed for 18 h at 580 K in flowing oxygen to activate its surfaces for dissociation of hydrogen molecules.[9] The nanocrystalline samples were used as produced, without any annealing treatment.

Ambient-temperature x-ray-diffraction measurements of samples $N1$, $N2$, and CG were made using nickel-filtered copper radiation ($\lambda=0.1542$ nm for copper $K\alpha$) produced by a 2-kW tube source operated at 45 kV and 30 mA. A standard Rachinger correction[17] was applied to the data to account for asymmetric intensity-peak shapes due to the presence of strong $K\alpha_1$ and $K\alpha_2$ components of differing intensities. Scans (θ-2θ) were collected in reflection mode with the scattering vector aligned approximately perpendicular to the sample surface. A scintillation detector was used, with typical counting times of 40–200 s and step sizes of 0.08° (2θ). For sample $N1$, x-ray data were typically collected over the angular range $2\theta=30°-100°$, such that the first five Bragg peaks were sampled (111–222). A wider angular range $2\theta=30°-130°$ was scanned for samples $N2$ and CG such that the eight Bragg peaks up to and including (420) were observed.

The samples were mounted inside a cryostat used in this experiment as a room-temperature controlled-environment chamber. Steps in the typical data-collection procedures included (1) placing the sample into the environmental chamber, (2) evacuating the sample surroundings to a pressure of approximately 1.3×10^{-4} Pa, (3) collecting a scan from the sample prior to any hydrogen exposure, (4) backfilling the sample surroundings with a desired pressure of hydrogen, and (5) collecting x-ray scans during and following incorporation of hydrogen into the sample. Steps (4) and (5) were repeated at several hydrogen pressures for each sample.

The samples were exposed to hydrogen at pressures less than or equal to 1 atm. Most scans were obtained at pressures of 0–6 kPa. For samples $N1$, $N2$, and CG, hydrogen-pressure–composition relationships were determined for pressures below the minimum required to induce the transformation to the hydride phase. From these data an estimate could be made of the Sievert's constant k in the relationship $\mathrm{H/Pd}=kp^{1/2}$, where H/Pd is the hydrogen concentration in the sample and p is pressure.[9] The minimum hydrogen pressure required to induce the α-to-β phase transition at room temperature was also noted for these three samples. For sample $N1$ only, the hydrogen was removed from the sample by evacuating the cryostat each time the hydrogen pressure was changed. For samples $N2$ and CG, the hydrogen pressure in the cryostat was increased or decreased stepwise by simply increasing or decreasing the hydrogen pressure in the sample chamber.

X-ray data from sample $N3$ were obtained at the National Synchrotron Light Source (NSLS) using Beamline X7A. In this case, x rays of wavelength $\lambda=0.078\,48$ nm were selected using a Ge(111) monochromator. This sample was also mounted in a cryostat so that it could be exposed to a controlled pressure of gaseous hydrogen. Data were acquired using a straight-wire position-sensitive detector (PSD). The PSD spanned approximately 6.5°, but only the central 2.6° were used because of an observed sensitivity variation along the wire. A linear correction factor was applied to correct the intensities in the retained portion of the spectra. The PSD was used to obtain θ-2θ scans with step sizes of 2.0° and counting times at each position of 60 s. Data were collected over an angular range of $2\theta=28°-68°$, such that the eight Bragg peaks from (220) to (511,333) were sampled.

Because of beam-time limitations, sample $N3$ was not allowed to equilibrate at several hydrogen pressures below and above the transition pressure, as was done for the other samples in this study, but instead was exposed only to a pressure significantly above that needed to induce the α-to-β transformation. This sample was held at 300 K and a pressure of 10 kPa. Scans were acquired repeatedly as it transformed to β-PdH. This procedure allowed a determination of the phase boundaries of the miscibility gap at 300 K, as discussed below, but not a determination of the minimum hydrogen pressure required to induce the α-β phase transition or a determination of the hydrogen-pressure–concentration dependence for this sample. Sample $N3$ was also thoroughly characterized prior to hydrogen exposure in two other x-ray-diffraction studies.[7,8] Following its complete transformation to the β-PdH phase, the sample was cooled rapidly to 40 K and then scanned at several temperatures from 40 to 300 K to determine the thermal properties of nanocrystalline β-PdH. The results of the temperature study will be published separately.[18]

The x-ray data obtained in this study were analyzed using kinematical x-ray-diffraction theory, as described in Ref. 8. In this analysis the locations of the intensity peaks for each sample and hydrogen pressure were determined by χ^2 minimization techniques.[19] From this infor-

mation the lattice parameters of the samples were obtained as a function of hydrogen pressure. Both α-PdH and β-PdH have a face-centered-cubic (fcc) structure with hydrogen occupying octahedral sites in the palladium lattice.[20] As the hydrogen concentration in the α-PdH phase increases, the lattice dilates and the α-PdH reflections move to smaller 2θ (larger d spacings). A second set of Bragg reflections appears at smaller angles when the β-PdH phase begins to form. Hydrogen concentrations in the samples were determined by making use of the known linear increase in the lattice parameter of palladium with increasing hydrogen concentration,[21,22] according to

$$\frac{3}{a_0}\frac{\Delta a_0}{\Delta x}=0.19\pm0.01\ , \tag{1}$$

where a_0 is the lattice parameter and $x=\mathrm{H/Pd}$ is the hydrogen concentration. This relationship has been shown to hold for $\mathrm{H/Pd}<0.7$ (Ref. 21) and thus can be used to determine both $\alpha_{\max}$ and $\beta_{\min}$ at room temperature. While the sample is in the two-phase regime, the positions of both sets of reflections are invariant, but the relative intensities of one set of reflections increase as the other set decreases in intensity. The $\alpha_{\max}$ and $\beta_{\min}$ concentrations are thus determined by measuring the lattice parameters of both phases in the two-phase regime and then using Eq. (1) to convert changes in the lattice parameter into changes in composition.

Following the x-ray experiment, the hydrogen was removed from the samples by evacuating the sample surroundings, and transmission electron microscopy (TEM) was then used to determine the grain-size distributions in nanocrystalline samples $N2$ and $N3$. The microstructure of a sample cut from the same heat-treated coarse-grained palladium sheet as sample CG was also observed using TEM. TEM samples were prepared by electropolishing with a nonacid solution, BK-2,[23] at $-20\,^{\circ}\mathrm{C}$, 225 V, and 40 mA. Bright- and dark-field images and selected-area diffraction patterns were obtained using a JEOL 100 CX microscope operated at 100 keV.

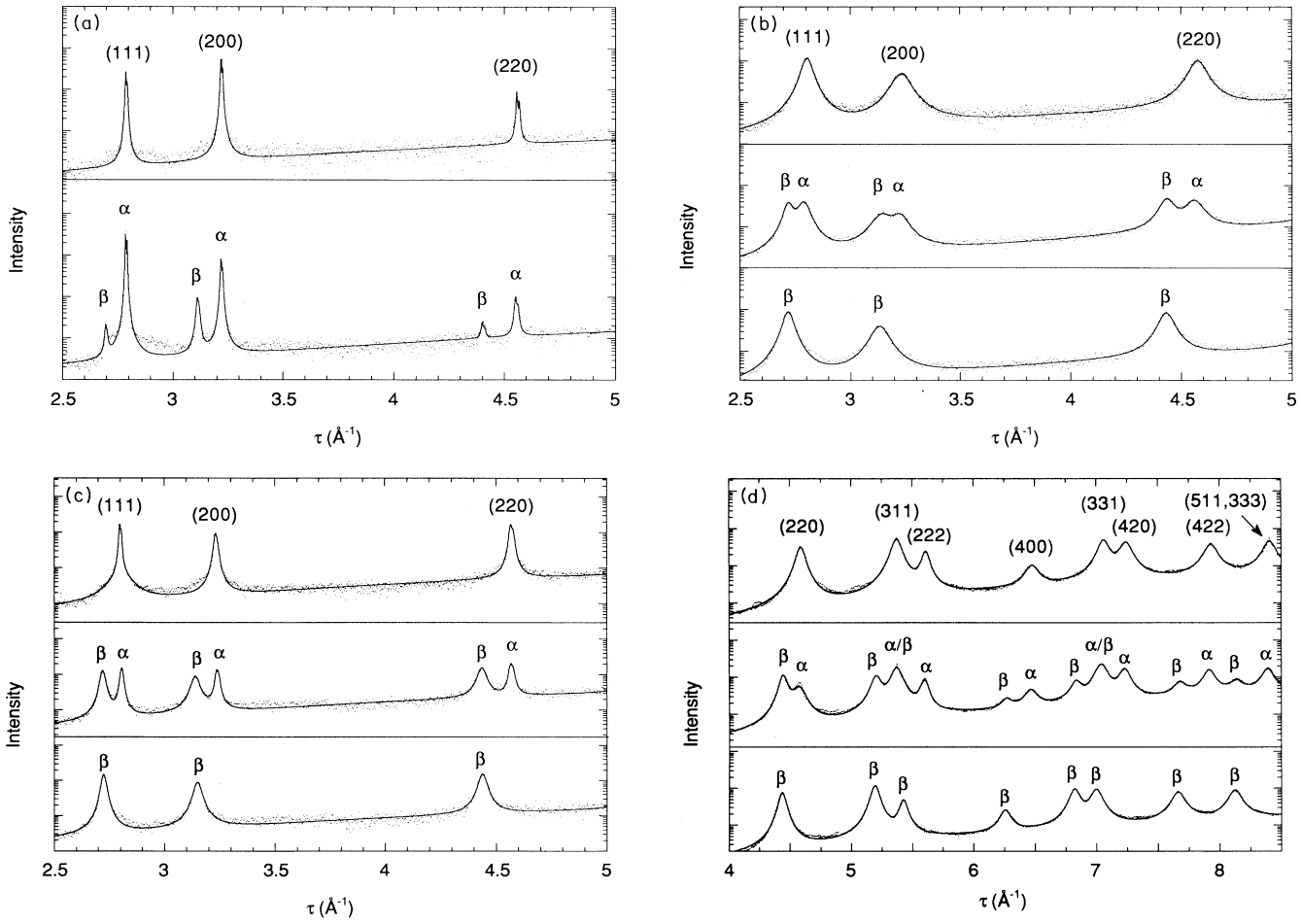

FIG. 1. Diffracted x-ray intensity plotted vs scattering vector magnitude, $\tau=4\pi\sin\theta/\lambda$. The solid curves indicate the best fit to the data. (a) Coarse-grained Pd prior to any hydrogen exposure (top) and in the mixed-phase regime (bottom). (b) Nanocrystalline sample $N1$ prior to any hydrogen exposure (top), during the transformation from α-PdH to β-PdH (middle), and after complete conversion of the sample to the β-PdH phase (bottom). (c) and (d) are the same as (b) for samples $N2$ and $N3$, respectively.

III. RESULTS

Plots of diffracted x-ray intensity versus scattering vector τ, where $\tau=4\pi\sin\theta/\lambda$, are shown in Fig. 1 for the four samples examined in this study. The solid curves in each case represent the best fit to the data. In Fig. 1(a) the τ range containing the first three Bragg peaks is seen for sample CG prior to any hydrogen exposure (top) and following exposure to hydrogen for 10 days (bottom). The hydrogen pressure during this time had been increased in eight increments from 0 to 5 kPa. This exposure resulted in a partial transformation of the coarse-grained sample to the β-PdH phase, as evidenced by the expected appearance of additional intensity peaks at smaller τ than that of the original palladium peaks. Although the coarse-grained sample had been annealed in oxygen to activate its surfaces for dissociation of hydrogen molecules,[9] it was found to be impossible to convert this sample completely to the hydride phase at room temperature, even after exposure to 1 atm of hydrogen for 3 weeks. This is not surprising, since it is well known that the hydrogen dissociation reaction can easily be poisoned at room temperature by adsorption of surface contaminants.[9] The transformation observed was sufficient, however, for determining the change in the α-phase lattice parameter with increasing hydrogen pressure, as well as the lattice parameters of the α and β phases in the mixed-phase regime (α_{max} and β_{min}), which are the parameters that correspond to the phase boundaries of the miscibility gap.

Diffraction scans from the three nanocrystalline samples $N1$, $N2$, and $N3$ are shown in Figs. 1(b), 1(c), 1(d) respectively. In each case the top scan was acquired from the sample prior to any exposure to hydrogen, the middle scan was obtained in the mixed-phase regime during transformation from α-Pd to β-PdH, and the bottom scan is from the same sample following complete conversion to the β-PdH phase. For all three samples, it was observed that the α-PdH intensity peaks were completely transformed to β-PdH intensity peaks after exposure to hydrogen at room temperature for times of less than 1 day at pressures above the minimum hydrogen pressure required to induce the α-to-β phase transition. This apparent improved resistance to poisoning of the hydrogen dissociation reaction for nanocrystalline palladium compared to coarse-grained palladium is consistent with simi-

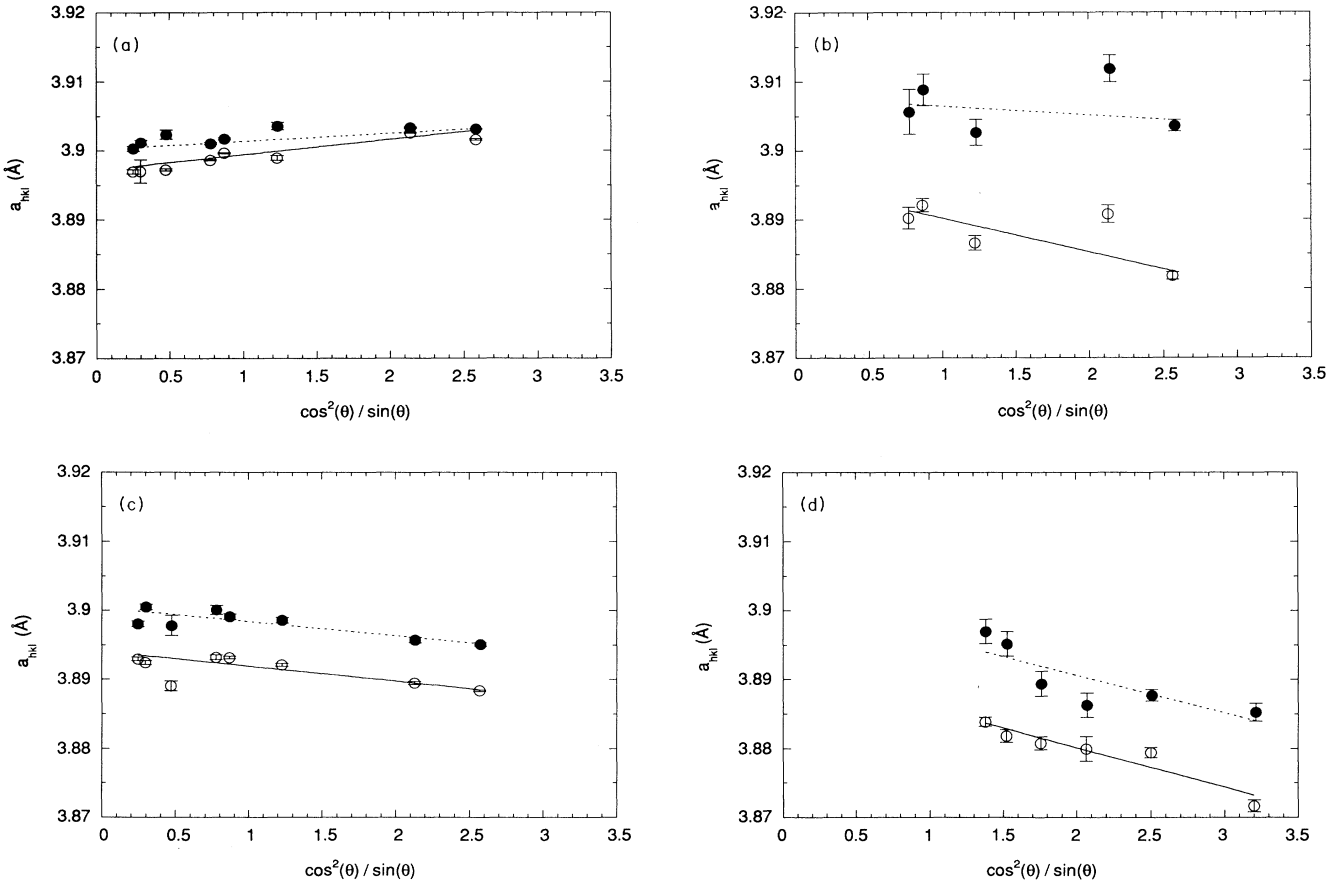

FIG. 2. Apparent lattice parameter for each intensity peak vs the $\cos^2(\theta)/\sin(\theta)$ extrapolation function prior to any hydrogen exposure (○) and at α_{max} (●). (a) Sample CG, (b) sample $N1$, (c) sample $N2$, and (d) sample $N3$.

TABLE I. Lattice-parameter data and corresponding hydrogen concentrations.

Sample	Lattice parameter (Å) Pd	Pd-H (α_{max})	Pd-H (β_{min})	Hydrogen concentration (H/Pd) α_{max}	β_{min}
CG	3.8972±0.0009	3.9006±0.0003	4.0387±0.0019	0.014±0.004	0.573±0.030
$N1$	3.8952±0.0015	3.9079±0.0020	4.0167±0.0024	0.052±0.010	0.493±0.028
$N2$	3.8943±0.0008	3.9014±0.0008	4.0220±0.0031	0.029±0.004	0.518±0.030
$N3$	3.8917±0.0010	3.9018±0.0021	4.0208±0.0030	0.041±0.009	0.524±0.030

lar reported improvements for coarse-grained samples coated with a thin layer of ultrafine palladium powder (palladium black).[9]

Lattice parameters were derived by measuring intensity-peak positions and plotting the apparent lattice parameters for each intensity peak versus $\cos^2\theta/\sin\theta$. This procedure is recommended for removing possible error due to specimen displacement from the axis of rotation.[24] The actual lattice parameter of a sample was obtained by extrapolating a linear fit through the data points to $\cos^2\theta/\sin\theta=0$ ($\theta=90°$). Lattice parameters prior to hydrogen exposure and at α_{max} were derived from Figs. 2(a), 2(b), 2(c), and 2(d) for samples CG, $N1$, $N2$, and $N3$, respectively. In Figs. 3(a)–3(d) the lattice parameters prior to hydrogen exposure and at β_{min} are shown, again for samples CG, $N1$, $N2$, and $N3$. The lattice parameters from Figs. 2 and 3 are given in Table I along with the hydrogen concentrations derived using Eq. (1).

A comparison of the miscibility-gap phase boundaries obtained from the present data with values from the literature[3,22,25,26] is seen in Fig. 4. The coarse-grained data points from the present study show a slightly narrower room-temperature miscibility gap than the literature values. The phase-boundary compositions for the nanocrystalline samples indicate a significant narrowing of the miscibility gap compared to both the literature values and the present coarse-grained data. In the present case, the α_{max} concentrations for the nanocrystalline samples increased by 200–370 %, while the β_{min} con-

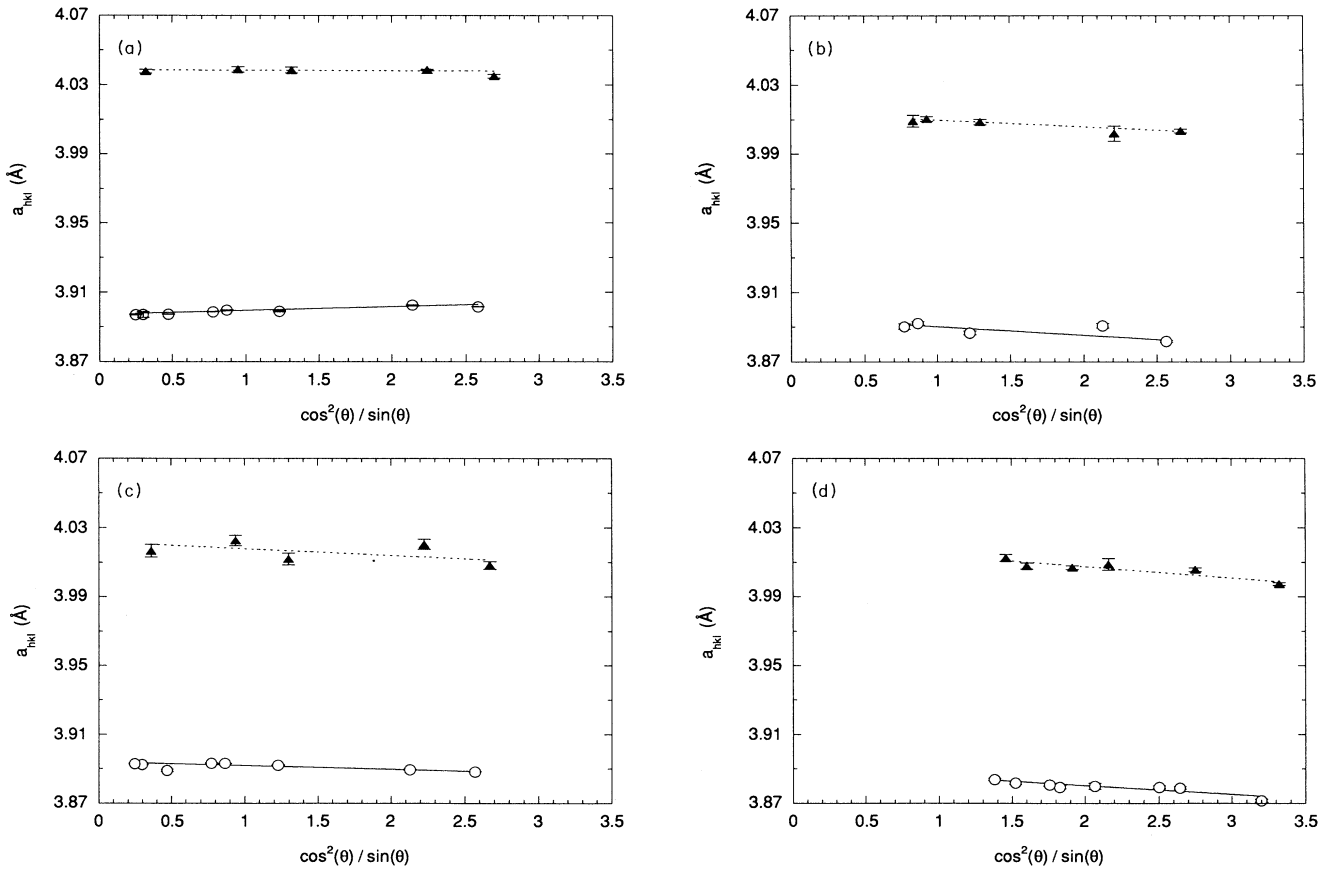

FIG. 3. Apparent lattice parameter for each intensity peak vs the $\cos^2(\theta)/\sin(\theta)$ extrapolation function prior to any hydrogen exposure (○) and at β_{min} (▲). (a) Sample CG, (b) sample $N1$, (c) sample $N2$, and (d) sample $N3$.

centrations decreased by 9–14% compared to the coarse-grained sample. This is in qualitative agreement with the observations of Mütschele and Kirchheim.[3]

The hydrogen-pressure–concentration dependences in the α phase were determined for samples $N1$, $N2$ and CG and are plotted in Fig. 5. Literature values[27] for coarse-grained palladium at 303 and 363 K are also plotted for comparison. Sievert's constant is obtained from the slope of a linear fit to the data in this figure. The values of Sievert's constant derived for samples CG, $N1$, and $N2$ are given in Table II along with the literature values for coarse-grained samples at three temperatures.[27] Sievert's constant for the coarse-grained sample of the present study at room temperature was found to be approximately 30% smaller than the literature value for coarse-grained palladium at 303 K. The two nanocrystalline samples have Sievert's constants that are 2.2 ($N2$) and 3.7 ($N1$) times larger than that of the coarse-grained sample at the same temperature.

TABLE II. Sievert's constant $k=(\mathrm{H/Pd})/p^{1/2}$, for samples $N1$, $N2$, and CG from the present study, compared with literature values (Ref. 27) for coarse-grained palladium at 273, 303, and 363 K.

Sample	k ($\mathrm{kPa}^{-1/2}$)
$N1$	0.0223±0.0020
$N2$	0.0127±0.0008
CG	0.0059±0.0002
273 K[a]	0.0123
303 K[a]	0.0084
363 K[a]	0.0044

[a]Reference 27.

The minimum hydrogen pressure required to induce the α-to-β phase transition to occur at room temperature was observed to be larger for nanocrystalline sample $N1$ than for either sample $N2$ or the coarse-grained sample CG. Values of 2.9±0.3 kPa for sample CG, 4.7±0.4 kPa for sample $N1$, and 3.3±0.4 kPa for sample $N2$ were obtained. The literature value for coarse-grained palladium at 303 K is 2.4 kPa.[9]

Dark-field TEM images were used to construct grain-size histograms of the nanocrystalline samples. Sample $N3$ was observed to have a median grain size of 8.3 nm.[8] Because of extensive cracking of sample $N1$ as a result of the hydriding experiment, TEM samples could not be successfully prepared from this sample. However, an analysis of the width of x-ray intensity peaks indicated that samples $N1$ and $N3$ were very similar in terms of both grain-size and strain distributions and thus sample $N1$ is also believed to have had a mean grain size of approximately 8 nm. Sample $N2$ was found to contain a bimodal grain-size distribution. As seen in Fig. 6, this sample contained nanocrystalline regions also having a mean grain size of approximately 8 nm, as well as other regions that contained micrometer-sized grains. An analysis of the x-ray intensity-peak breadths in Fig. 1(c) indicated

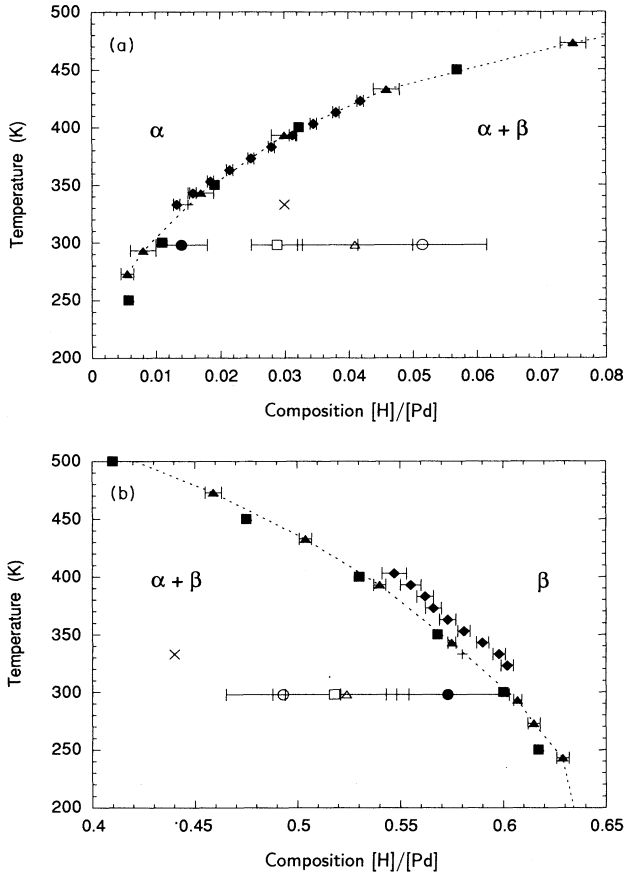

FIG. 4. (a) Low- and (b) high-hydrogen-concentration portions of the miscibility gap in the Pd-H phase diagram. The phase-boundary positions derived in the present study for samples CG (●), $N1$ (○), $N2$ (□), and $N3$ (△) are compared with the results of Mütschele and Kirchheim (Ref. 3) for coarse-grained (+) and nanocrystalline (×) Pd at 333 K and with literature results for the phase boundaries in coarse-grained Pd given by Kuji *et al.* (Ref. 25) (■), Wicke, Brodowsky, and Züchner (Ref. 22) (▲), and Lässer (Ref. 26) (◆).

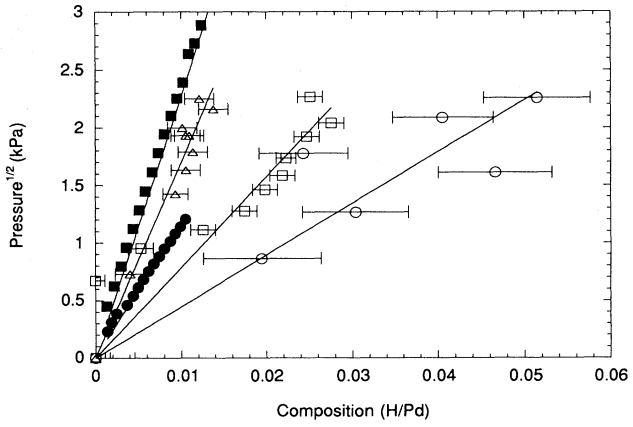

FIG. 5. Square root of the hydrogen pressure vs composition for samples $N1$ (○), $N2$ (□), and CG (△). Lines representing fits to the data points for coarse-grained palladium at 303 K (●) and 363 K (■) are also shown for comparison.

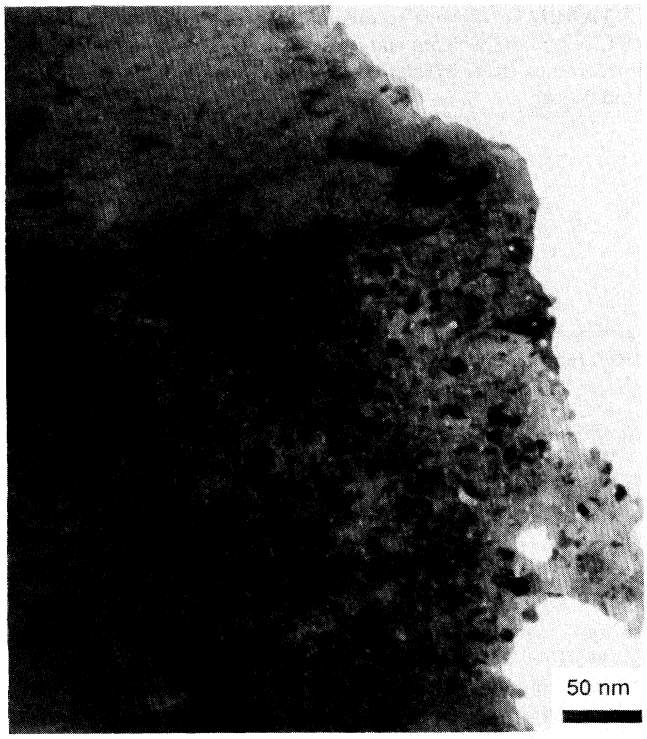

FIG. 6. (a) Bright-field and (b) dark-field TEM micrographs from sample $N2$ indicating the presence of a bimodal grain-size distribution. Grains with an average size of approximately 8 nm are seen in the lower portion of the figures, while micrometer-sized grains are seen in the upper portion of the figures.

that the bimodal grain-size distribution was present in sample $N2$ prior to any hydrogen exposure and thus was not caused by the hydriding that preceded the TEM observations. This type of bimodal grain-size distribution has been seen in other nanocrystalline palladium samples.[7] Whether the large-grained regions in sample $N2$ were due to subtle differences in the sample production process or were due to post-production room-temperature grain growth in portions of the sample is not known. The coarse-grained sample CG had a grain size larger than the $\sim 50 \times 50$ μm^2 electron transparent area in this sample, indicating that the grain size of this sample was at least three to four orders of magnitude larger than that of samples $N1$ and $N3$.

IV. DISCUSSION

Mütschele and Kirchheim[3] proposed that the decrease in β_{min} concentration in nanocrystalline palladium is due to the presence of disordered grain-boundary regions that cannot be transformed to the hydride phase. If grain boundaries in nanocrystalline materials had highly disordered structures as suggested, this would result in increased diffuse background intensities in x-ray-diffraction scans since the grain-boundary volume in these materials is a significant fraction of the total sample volume. However, recent quantitative comparisons of nanocrystalline and coarse-grained palladium samples revealed no significant grain-size-dependent differences in x-ray background intensities, indicating that the grain-boundary regions in nanocrystalline Pd scatter into the intensity peaks.[7,8] The present observation that α-phase x-ray intensity peaks from nanocrystalline samples are completely transformed to β-phase peaks after hydrogen exposure demonstrates that the entire volume of nanocrystalline palladium samples, including the grain-boundary regions, transforms to the hydride phase. This again indicates that there is no large disordered volume in nanocrystalline palladium samples, and therefore the explanation offered by Mütschele and Kirchheim to explain their observations cannot be correct.

The fact that the narrowing of the miscibility gap can be observed by measuring changes in the x-ray intensity-peak position is further evidence that the microstructural features responsible for the change in the palladium-hydrogen phase diagram have structural order that produces x-ray intensity peaks at normal Bragg positions rather than simply diffuse background intensity as would be expected from a highly disordered structure.

An alternative explanation for this difference in behavior of nanocrystalline and coarse-grained palladium can be proposed by examining the thermodynamics of systems containing a miscibility gap. The free energy of mixing, ΔG_m, is given by $\Delta G_m = \Delta H_m - T\Delta S_m$, where ΔH_m is the enthalpy of mixing, T is the temperature, and ΔS_m is the entropy of mixing. Since ΔS_m is always a positive quantity,[28] a miscibility gap occurs only when ΔH_m is positive and sufficiently large.[28] The free-energy of mixing components for a system containing a miscibility gap are shown qualitatively in Fig. 7(a), which for simplicity is drawn for the case of a regular solution. Curves in

this figure designated A and B represent two possible energy states of the system at constant ΔH_m. The compositions of the miscibility-gap phase boundaries are denoted a and b for energy state A, and c and d for energy state B.

One way of narrowing the miscibility gap shown in Fig. 7(a) from the phase-boundary compositions corresponding to state A to that of state B is to increase the temperature while keeping ΔS_m and ΔH_m constant. This is the normal temperature behavior of the Pd-H miscibility gap, which, for coarse-grained or single-crystal samples, narrows with increasing temperature until a critical temperature of 570 K is reached.[9]

In the present case the width of the Pd-H miscibility gap differs for coarse-grained and nanocrystalline Pd at constant temperature. This indicates that ΔS_m and/or ΔH_m differ in nanocrystalline and coarse-grained samples. Qualitatively, from Fig. 7(a), it can be seen that a larger ΔS_m at constant temperature and ΔH_m could yield

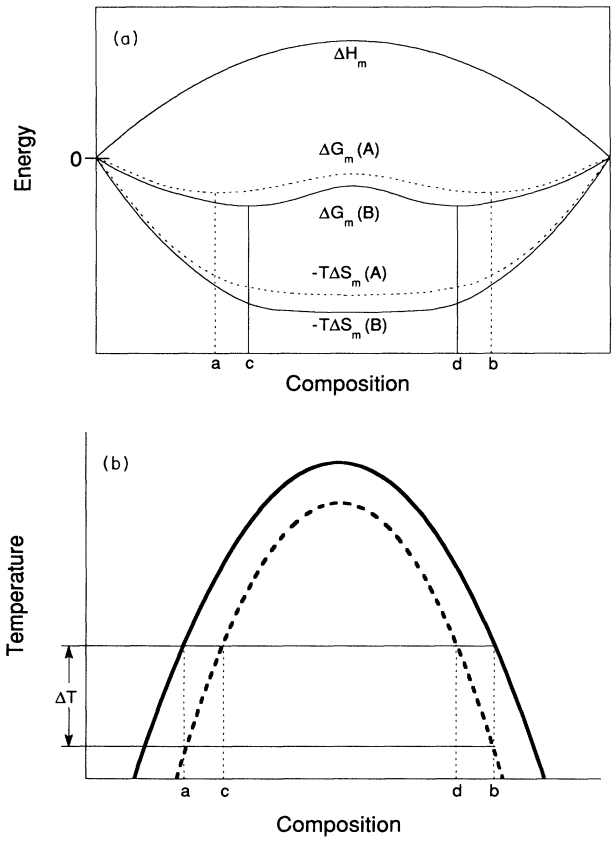

FIG. 7. Qualitative form of an energy-composition diagram for a system containing a miscibility gap. Curves designated A and B represent two possible energy states of the system. Energy state B exhibits a narrower miscibility gap than that for A, as a result in this illustration of either a higher temperature or larger ΔS_m at constant ΔH_m. (b) A schematic description of the predicted effect of reducing grain size on the palladium-hydrogen miscibility gap. The dashed curve represents the phase boundary for nanocrystalline palladium, while the solid curve is the phase boundary for conventional coarse-grained material.

the same narrowing of the miscibility gap that a temperature increase at constant ΔS_m and ΔH_m produces. The present results indicate that the ratio ΔS_m:ΔH_m must be larger for a nanocrystalline sample than for a coarse-grained one, but it is not possible to tell from these data whether both or only one of these quantities change, or even whether they increase or decrease in magnitude. For example, both quantities could increase in magnitude if ΔS_m increases more than ΔH_m. Likewise, both could decrease in magnitude as long as ΔS_m decreases less than ΔH_m.

Nanocrystalline materials have been shown to possess different thermodynamic properties compared to those in coarse-grained or single-crystal materials.[29] To date, however, there have been no reported measurements or calculations of enthalpies or entropies of mixing for nanocrystalline solutions. Since atoms have different surroundings in grain-boundary regions than in grain interiors, it is conceivable that grain boundaries exhibit different thermodynamic mixing quantities than perfect crystal regions. These differences would not have a detectable effect on the width of a miscibility gap in normal coarse-grained samples where the total grain-boundary volume is insignificant, but could modify the behavior of nanocrystalline materials where grain boundaries constitute a large volume fraction of the material.

The large strain distributions known to be present in nanocrystalline materials[7,8] could also lead to significant changes in thermodynamic properties and thus be responsible for the observed changes in the Pd-H miscibility gap. Since these strains are observed in unconsolidated nanocrystalline powders prepared by the gas-condensation techniques used in the present experiment, as well as in compacted samples, the strains are not necessarily associated with grain boundaries, but may instead result from defects produced during the powder production process. Strain in coarse-grained samples has previously been associated with enhancements of ambient-temperature α-phase hydrogen solubility,[30,32] but there have been no reports of reductions in the $\beta_{\min}$ concentration in strained samples. It is not clear whether this effect has been investigated, however.

A narrowing of the Pd-H miscibility gap in nanocrystalline samples due to an increase in the ratio ΔS_m:ΔH_m would shift the phase boundary to lower temperatures at constant composition and reduce the critical temperature, as shown qualitatively in Fig. 7(b). The present data indicate that the palladium-hydrogen miscibility-gap phase boundary for the three observed nanocrystalline samples is lowered by $\Delta T = 70° - 100°$ compared to that for coarse-grained palladium. Repeating the experiment at several temperatures with different grain-sized samples and different strain contents would be necessary to determine the detailed dependence of the miscibility gap on these variables. Reports of reduced melting temperatures for nanometer-grain-sized thin films of lead, tin, and bismuth[33] and small particles of gold[34] are other examples of known reductions in phase-transformation temperatures with increasing interfacial area.

While the present results indicate that both decreasing grain size and increasing temperature affect the Pd-H

phase diagram in the same way, these two variables have opposite effects on the pressure-composition diagram shown in Fig. 5. For fixed grain size, an increasing temperature results in a diminished α-phase solubility at constant pressure.[27] In contrast, the present results indicate that decreasing grain size at fixed temperature increases solubility. This is consistent with grain boundaries having a higher hydrogen solubility than the bulk.[3]

V. CONCLUSIONS

The present results demonstrate that the narrowing of the palladium-hydrogen miscibility gap is associated with a larger ratio of the value of the entropy of mixing to that of the enthalpy of mixing in nanocrystalline samples than in coarse-grained samples. Grain boundaries and/or strain may be responsible for these changes in thermodynamic quantities. The resulting effect on the phase diagram is to shift the miscibility-gap phase boundary to lower temperature for nanocrystalline material. This interpretation is consistent with the present observations that nanocrystalline samples could be completely transformed to the hydride phase, as well as with previous reports indicating that the grain-boundary regions in nanocrystalline palladium are not highly disordered compared with boundaries in normal coarse-grained palladium.

ACKNOWLEDGMENTS

This work was supported by the U.S. Department of Energy, BES-Materials Sciences, under Contract No. W-31-109-Eng-38. We gratefully acknowledge useful discussions with Charlie Allen and Paul Okamoto. We thank Mike Fitzsimmons and Dr. D. Cox for their assistance in acquiring the data from sample *N*3. The National Synchrotron Light Source, Brookhaven National Laboratory, is supported by the U.S. Department of Energy, Division of Materials Sciences and Division of Chemical Sciences.

[1]H. Gleiter, Prog. Mater. Sci. **33**, 223 (1989).
[2]R. P. Andres *et al.*, J. Mater. Res. **4**, 704 (1989).
[3]T. Mütschele and R. Kirchheim, Scr. Metall. **21**, 1101 (1987).
[4]X. Zhu, R. Birringer, U. Herr, and H. Gleiter, Phys. Rev. B **35**, 9085 (1987).
[5]T. Haubold, R. Birringer, B. Lengeler, and H. Gleiter, J. Less-Common Met. **145**, 557 (1988).
[6]G. J. Thomas, R. W. Siegel, and J. A. Eastman, Scr. Metall. Mater. **24**, 201 (1990).
[7]M. R. Fitzsimmons, J. A. Eastman, M. Müller-Stach, and G. Wallner, Phys. Rev. B **44**, 2452 (1991).
[8]J. A. Eastman, M. R. Fitzsimmons, and L. J. Thompson, Philos. Mag. B **66**, 667 (1992).
[9]F. A. Lewis, *The Palladium Hydrogen System* (Academic, London, 1967).
[10]R. Griessen, Phys. Rev. B **27**, 7575 (1983).
[11]J. A. Eastman, M. R. Fitzsimmons, M. Müller-Stach, G. Wallner, and W. T. Elam, J. Nanostruct. Mater. **1**, 47 (1992).
[12]K. Kimoto, J. Phys. Soc. Jpn. **8**, 762 (1953).
[13]K. Kimoto, Y. Kamilaya, M. Nonoyama, and R. Uyeda, Jpn. J. Appl. Phys. **2**, 702 (1963).
[14]C. G. Granqvist and R. A. Buhrman, J. Appl. Phys. **47**, 2200 (1976).
[15]H. Gleiter, in *Deformation of Polycrystals: Mechanisms and Microstructures,* edited by N. Hansen *et al.* (Risø National Laboratory, Roskilde, Denmark, 1981), Vol. 15.
[16]*CRC Handbook of Chemistry and Physics,* 70th ed., edited by R. C. Weast, D. R. Lide, M. J. Astle, and W. H. Beyer (CRC, Boca Raton, FL, 1989), p. 27.
[17]B. E. Warren, *X-Ray Diffraction* (Dover, New York, 1990).
[18]J. A. Eastman, M. R. Fitzsimmons, and L. J. Thompson (unpublished).
[19]W. H. Press, B. P. Flannery, S. A. Teukolsky, and W. T. Vetterling, *Numerical Recipes* (Cambridge University Press, Cambridge, England, 1989).
[20]G. Nelin, Phys. Status Solidi B **45**, 527 (1971).
[21]B. Baranowski, S. Majchrzak, and T. B. Flanagan, J. Phys. F **1**, 258 (1971).
[22]E. Wicke, H. Brodowsky, and H. Züchner, in *Hydrogen in Metals II, Application-Oriented Properties,* edited by G. Alefeld and J. Völkl, Vol. 29 of *Topics in Applied Physics* (Springer-Verlag, Berlin, 1978), p. 73.
[23]B. J. Kestel, Ultramicroscopy **19**, 205 (1986).
[24]H. Lipson and H. Steeple, *Interpretation of X-Ray Powder Diffraction Patterns* (St. Martins, New York, 1970).
[25]T. Kuji, W. A. Oates, B. S. Bowerman, and T. B. Flanagan, J. Phys. F **13**, 1785 (1983).
[26]R. Lässer, J. Phys. Chem. Solids **46**, 33 (1985).
[27]J. W. Simons and T. B. Flanagan, J. Phys. Chem. **69**, 3773 (1965).
[28]Richard A. Swalin, *Thermodynamics of Solids* (Wiley, New York, 1961).
[29]H. J. Fecht, Acta Metall. Mater. **38**, 1927 (1990).
[30]T. B. Flanagan, J. F. Lynch, J. C. Clewley, and B. Von Turkovich, J. Less-Common Met. **49**, 13 (1976).
[31]J. F. Lynch, J. D. Clewley, T. Curran, and T. B. Flanagan, J. Less-Common Met. **55**, 153 (1977).
[32]R. V. Bucur, N. O. Ersson, and X. Q. Tong, J. Less-Common Met. **172-174**, 748 (1991).
[33]M. Takagi, J. Phys. Soc. Jpn. **9**, 359 (1954).
[34]Ph. Buffat and J.-P. Borel, Phys. Rev. A **13**, 2287 (1976).

(a)

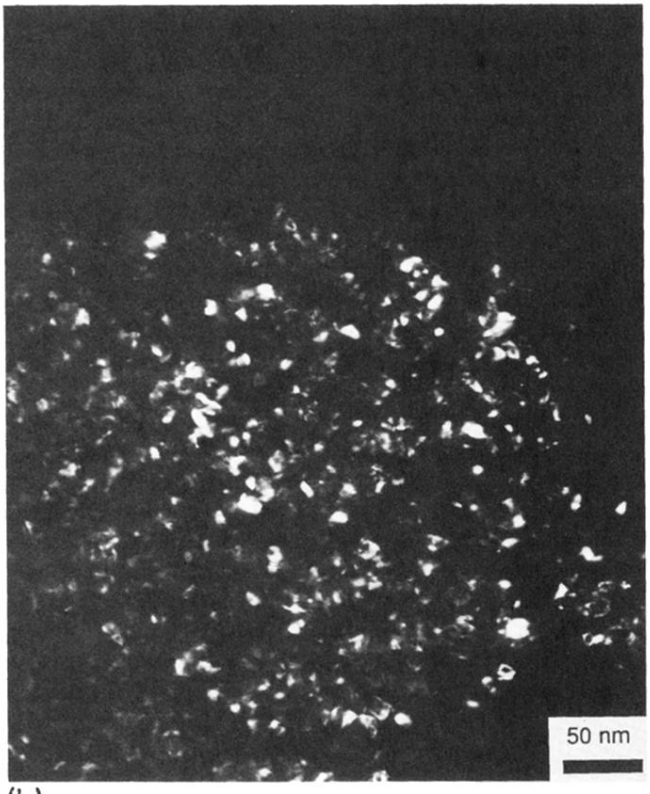

(b)

FIG. 6. (a) Bright-field and (b) dark-field TEM micrographs from sample $N2$ indicating the presence of a bimodal grain-size distribution. Grains with an average size of approximately 8 nm are seen in the lower portion of the figures, while micrometer-sized grains are seen in the upper portion of the figures.